Field-aligned distribution of the plasmaspheric electron density: An empirical model derived from the IMAGE RPI measurements

P. Ozhogin,[1,2] J. Tu,[1,2] P. Song,[1,2] and B. W. Reinisch[1,3]

Received 3 November 2011; revised 18 April 2012; accepted 17 May 2012; published 27 June 2012.

[1] We present a newly developed empirical model of the plasma density in the plasmasphere. It is based on more than 700 density profiles along field lines derived from active sounding measurements made by the radio plasma imager on IMAGE between June 2000 and July 2005. The measurements cover all magnetic local times and vary from L = 1.6 to L = 4 spatially, with every case manually confirmed to be within the plasmasphere by studying the corresponding dynamic spectrogram. The resulting model depends not only on L-shell but also on magnetic latitude and can be applied to specify the electron densities in the plasmasphere between 2000 km altitude and the plasmapause (the plasmapause location itself is not included in this model). It consists of two parts: the equatorial density, which falls off exponentially as a function of L-shell; and the field-aligned dependence on magnetic latitude and L-shell (in the form of invariant magnetic latitude). The fluctuations of density appear to be greater than what could be explained by a possible dependence on magnetic local time or season, and the dependence on geomagnetic activity is weak and cannot be discerned. The solar cycle effect is not included because the database covers only a fraction of a solar cycle. The performance of the model is evaluated by comparison to four previously developed plasmaspheric models and is further tested against the in situ passive IMAGE RPI measurements of the upper hybrid resonance frequency. While the equatorial densities of different models are mostly within the statistical uncertainties (especially at distances greater than L = 3), the clear latitudinal dependence of the RPI model presents an improvement over previous models. The model shows that the field-aligned density distribution can be treated neither as constant nor as a simple diffusive equilibrium distribution profile. This electron density model combined with an assumed model of the ion composition can be used to estimate the time for an Alfven wave to propagate from one hemisphere to the other, to determine the plasma frequencies along a field line, and to calculate the raypaths for high frequency waves propagating in the plasmasphere.

Citation: Ozhogin, P., J. Tu, P. Song, and B. W. Reinisch (2012), Field-aligned distribution of the plasmaspheric electron density: An empirical model derived from the IMAGE RPI measurements, *J. Geophys. Res.*, *117*, A06225, doi:10.1029/2011JA017330.

1. Introduction

[2] The plasmasphere is the high altitude extension of the ionosphere and consists of cold (temperature ~1 eV), dense (density 10^2–10^4 cm^{-3}) plasma. It is a highly dynamic region that contains density structures of various spatial scales. The plasmasphere plays a profound role in space weather. Its density distributions and their time variations determine the characteristics of the plasma waves (e.g., hiss, chorus, EMIC) within the plasmasphere and affect the propagation of those waves, as well as magnetohydrodynamic (MHD) waves, which in turn influence the radiation belt dynamics. Therefore, it is necessary to study the plasmasphere density distribution and to develop reliable empirical models of the plasmasphere density. Such models are important since they help with the investigation of wave propagation in the plasmasphere, with modeling the radiation belt, and with forecasting space weather. Furthermore, the empirical models can be used as a benchmark for the theoretical and numerical modeling [*Siscoe et al.*, 2004], or as a gauge of the density fluctuations during periods of geomagnetic disturbances [*Reinisch et al.*, 2004]. Additionally, these models can be used to assess the refilling rates of the plasmasphere and/or plasmatrough [*Singh and Horwitz*, 1992; *Rasmussen et al.*, 1993; *Lawrence et al.*, 1999;

[1]Center for Atmospheric Research, University of Massachusetts Lowell, Lowell, Massachusetts, USA.
[2]Physics Department, University of Massachusetts Lowell, Lowell, Massachusetts, USA.
[3]Lowell Digisonde International, LLC, Lowell, Massachusetts, USA.

Corresponding author: P. Ozhogin, Center for Atmospheric Research, University of Massachusetts Lowell, 600 Suffolk St., Lowell, MA 01854, USA. (ozhogin@gmail.com)

©2012. American Geophysical Union. All Rights Reserved.
0148-0227/12/2011JA017330

Tu et al., 2006]. For example, an empirical model may represent the plasmasphere in an averagely filled state. As shown by *Reinisch et al.* [2004], the plasmaspheric density can be substantially depleted during a magnetic storm and it would take less than 28 h for the plasmasphere to refill to the average level. This time scale may be used to estimate the refilling time.

[3] The efforts of developing empirical models that statistically describe the plasmasphere morphology date back to the 1960s, when *Binsack* [1967] established an empirical relation of the plasmapause location with the K_p index by using in situ observations from the IMP 2 satellite. Later on, whistler observations conducted both on the ground and on ISEE 1 spacecraft as well as in situ measurements from DE 1 and CRRES satellites were used to develop more sophisticated empirical plasmapause models [*Carpenter and Anderson*, 1992; *Moldwin et al.*, 2002; *O'Brien and Moldwin*, 2003]. In parallel to the modeling of the plasmapause location, empirical models of the equatorial density have also been developed with whistler observations, in situ probing, radio wave remote measurements, and extreme ultraviolet (EUV) imaging [e.g., *Carpenter and Anderson*, 1992; *Sheeley et al.*, 2001; *Denton et al.*, 2004; *Reinisch et al.*, 2004; *Song et al.*, 2005; *Tu et al.*, 2006; *Larsen et al.*, 2007]. Moreover, efforts have been made to statistically represent the plasmasphere/plasmatrough density distributions off the equator by using the measurements from the above mentioned spacecraft [*Gallagher et al.*, 1988, 1998, 2000; *Goldstein et al.*, 2001; *Denton et al.*, 2004; *Huang et al.*, 2004; *Reinisch et al.*, 2004; *Tu et al.*, 2006].

[4] Despite the efforts over decades, our ability to accurately represent the plasmasphere density distribution is still limited. A major drawback is the lack of the models that can satisfactorily describe the off-equator density distribution globally [e.g., *Reinisch et al.*, 2009, and references therein]. The main reason is that the previous observations have been made in situ along the satellite orbits, and in limited locations under various geomagnetic activities. The averaging of these in situ data smoothes out the latitude-dependence of the density distribution, particularly density variation along individual magnetic field lines. It has been suggested theoretically that the plasmasphere density is in diffusive equilibrium [e.g., *Angerami and Thomas*, 1964]. With five varying parameters (ionic composition (H^+, He^+, O^+), temperature, and density at the base level) it is possible to create a wide variety of the field-aligned profiles. However, according to the diffusive equilibrium assumption, there is little dependence of the plasma density on latitude along individual magnetic field lines down to the altitude of $\sim$1 R_E. In other words, the density is almost constant in a large latitudinal range around the equator for a given field line (or *L*-shell) [e.g., *Gallagher et al.*, 2000]. However, the measurements from plasma wave instrument [*Gurnett et al.*, 1995] on the Polar spacecraft and, particularly, the radio plasma imager (RPI) [*Reinisch et al.*, 2000] on the IMAGE spacecraft have shown that density gradients along magnetic field lines are substantial and observable [*Goldstein et al.*, 2001; *Denton et al.*, 2002, 2004; *Huang et al.*, 2004; *Reinisch et al.*, 2004; *Song et al.,* 2005; *Tu et al.*, 2006].

[5] The IMAGE RPI measurements of the field-aligned electron density distribution are obtained almost instantaneously along the field line passed by the IMAGE spacecraft [see *Reinisch et al.*, 2001], adding to previous efforts in deriving the field-aligned electron density distributions that used limited density measurements made approximately on the same field line at different times [e.g., *Goldstein et al.*, 2001; *Denton et al.*, 2002, 2004, 2006]. The previous studies of the latitudinal dependence of the plasmasphere density using the IMAGE RPI active sounding measurements were conducted only for several plasmasphere passes by the IMAGE spacecraft [*Huang et al.*, 2004; *Reinisch et al.*, 2004; *Tu et al.*, 2006]. In the present study, we extend the IMAGE RPI investigations of the latitude-dependence by using a larger database consisting of more than 700 field-aligned density profiles derived from the RPI active sounding measurements. We develop a new empirical model of the plasmaspheric densities that describes the electron densities within the plasmasphere down to the altitude of $\sim$2000 km in both hemispheres. The significance of the model is that it depends not only on the *L*-shell, but also on the magnetic latitude (which has been suggested by *Huang et al.* [2004] based on several examples) producing a result consistent with a large number of RPI measurements. No evidence of the electron density increase at the equator has been found within the 700 plasmagrams. Such increase would produce a characteristic cusp-type feature of the echo traces that could not have been missed in our plasmagram trace analysis. However, the absence of such cusp-type signatures does not exclude the possibility of a mass density peak at the equator. In the following section we first briefly describe the RPI data and the method of constructing the empirical model. In section 3 we discuss how the present plasmasphere model is derived from the IMAGE RPI measurements. The model developed in the present study as well as previous models are evaluated by comparing the models with the RPI active sounding measurements and passive observations in section 4. Conclusions and a summary are given in the last section.

2. Data and Analysis Method

[6] The radio plasma imager (RPI) on the IMAGE satellite [*Burch*, 2000] has made unique and first of its kind remote measurements in the magnetosphere. The RPI instrument and measurement techniques have been described in detail by *Reinisch et al.* [2000]. The instrument is a low-power radar that performs active sounding in the frequency range from 3 kHz to 3 MHz and passive measurements in the range from 3 kHz to 1100 kHz. It is one of the six imaging instruments onboard IMAGE which revolved in an elliptical polar orbit (90 degrees inclination after launch, $\sim$7 R_E apogee altitude, and $\sim$1000 km perigee altitude). During active sounding measurements the RPI transmitted coded signals and listened to the response. The received signals resulted in "plasmagrams" illustrated in Figure 1, i.e., plots of amplitude of returned signal as a function of frequency (horizontal axis) and virtual range (time delay times half of the speed of light). During passive measurements, the RPI produced "dynamic spectrograms" as shown in Figure 2, plots of amplitude of a signal as a function of frequency (vertical axis) and time (horizontal axis), which reveal the plasma wave environment around the satellite. Plasmagrams obtained from the active soundings often contain discrete echo traces with enhanced signal strength. It has been shown

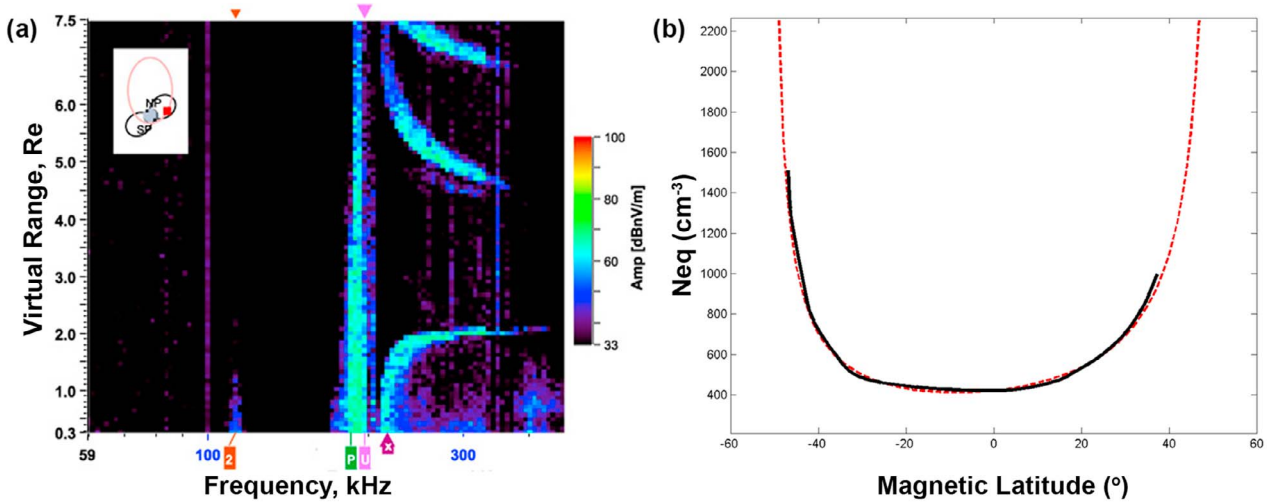

Figure 1. RPI measurements on 12 June 2002, 04:17 UT, MLT = 19.94, L = 2.94. (a) Plasmagram – color-coded echo amplitude as a function of frequency and virtual range in Earth radii made with BinBrowser [*Galkin et al.,* 2008]. The labels denote: second gyrofrequency harmonic, plasma and upper hybrid resonances, and local X mode cutoff frequency, respectively. The insert displays the IMAGE satellite orbit, with the satellite location marked by the red dot, and $L = 4$ field lines. (b) Electron density distribution as a function of magnetic latitude with solid line denoting the field-aligned density profile inverted from the traces shown in Figure 1a. The dashed red line is a least squares fit of the equation (1) to the RPI density profile, with $\alpha = 1.081$, $\beta = 0.678$ and $\gamma = 0.297$.

that these traces usually correspond to the reflected signals that propagate along the magnetic field line [e.g., *Reinisch et al.*, 2001; *Fung and Green*, 2005]. It is possible to invert such traces to derive the plasma densities along the individual magnetic field line with an inversion algorithm [*Huang et al.*, 2004] similar to that extensively used for the ionogram inversion [*Huang and Reinisch*, 1982; *Reinisch and Huang*, 1983]. The validation of the method has been documented in a few previous publications [e.g., *Reinisch et al.*, 2001]. In those case studies, multiple traces were measured for echoes of different paths and for different wave modes, and it was demonstrated that the echo signals propagated along the magnetic field lines. Then, the density distribution along the whole magnetic field line from one hemisphere to the other was derived using the X mode echo traces. The density profile was then used to predict the Z mode echo traces, and the results showed that the predictions are consistent with measurements. In other words, it is possible to reconstruct the traces, which are produced by both modes of propagation, from the derived density profile. This

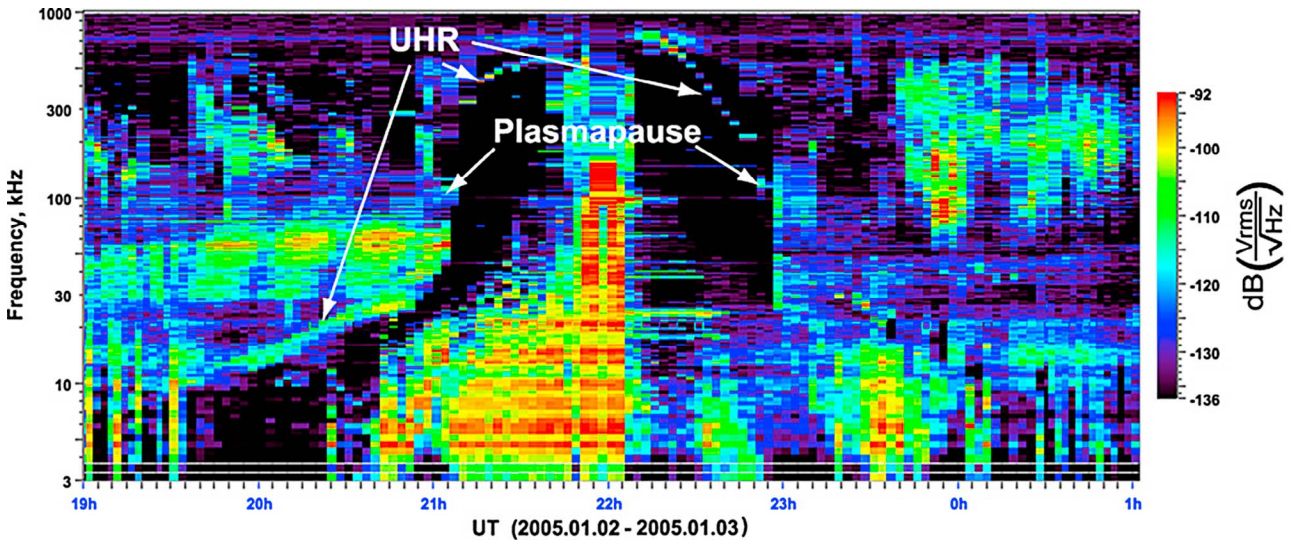

Figure 2. RPI dynamic spectrogram from 1900 UT on 1 January 2005 to 0100 UT on 2 January 2005. An upper hybrid resonance (UHR) noise band is clearly seen. Sharp decreases of frequency of the band around 2100 UT and 2300 UT indicate the plasmapause.

technique is much more accurate than, for example, the in situ density derived from the dynamic spectra because of the finer frequency resolution. Also this sounding technique avoids the ambiguity of the plasma frequency and the upper hybrid frequency, which often are very close to each other in the region of interest. The measurement uncertainty is much smaller than the natural variations of the density. Therefore, the conventional uncertainty due to instrumentation and inversion methodology is not a concern. The resulting density profile is an almost instantaneous snapshot of the density distribution along the field line since it is usually measured within less than 1 min (depending on the sounding program). Only from active RPI sounding measurements can we derive the field-aligned distribution of the density at a given time over the whole range of the latitudes, in contrast to the passive measurements that are in situ and cannot be used to determine the field-aligned distribution at a given time.

[7] A typical plasmagram obtained within the plasmasphere is shown in Figure 1a. Resonances at the local electron plasma frequency f_{pe}, upper hybrid resonance frequency f_{uh}, and electron gyrofrequency f_{ce}, are identified as vertical lines with enhanced signal strength. f_x is the X-mode cutoff frequency at the IMAGE location. Three echo traces are clearly seen in this case. The trace with the shortest virtual ranges consists of reflected signals propagating along the magnetic field line in the local hemisphere where the satellite is located; the second trace represents the echoes from the conjugate hemisphere; and the third trace denotes the signals that, after reflection in the local hemisphere, propagated to low altitudes in the conjugate hemisphere where they are reflected back to the satellite. By scaling the trace (thin lines overlap on the traces) and using a density inversion technique described in detail by *Huang et al.* [2004], we can derive an electron density profile (black line in Figure 1b). We then perform the least squares fit to the measured density profile using following expression [*Huang et al.*, 2004; *Reinisch et al.*, 2004; *Song et al.*, 2005] in order to determine the fitting parameters:

$$N(L,\lambda) = N_{eq}(L) \cdot \left(1 + \gamma \frac{\lambda}{\lambda_{INV}}\right) \cdot \cos^{-\beta}\left[\frac{\pi}{2} \cdot \frac{\alpha\lambda}{\lambda_{INV}}\right], \quad (1)$$

where L and λ_{INV} are the L-shell in units of Earth radius R_E, and the magnetic invariant latitude, respectively, of the geomagnetic field line on which the satellite made the measurements, and λ is the magnetic latitude on the field line. These values are calculated using the Tsyganenko 2001 (T01) [*Tsyganenko*, 2002] magnetospheric magnetic field model. Even though this model might be not much different from its earlier versions (or even a simple dipole model) close to Earth, there are differences at larger distances, especially during the cases of moderate or high geomagnetic activity. The use of T01 throughout the whole database is done in order to maintain consistency in the results and avoid the variations due to multiple magnetic field models. N_{eq} is the equatorial density. It has been shown in previous studies that the functional form of equation (1) well represents the field-aligned density profiles in the filled plasmasphere on the dayside [*Huang et al.,* 2004; *Reinisch et al.*, 2004; *Song et al.*, 2005], as well as the field-aligned density profiles along both the filled and depleted flux tubes around local midnight [*Tu et al.*, 2006]. Expression (1) has been developed empirically based on a large number of profiles and it provides extremely good fits for the majority of the cases (average relative error is less than 10%).

[8] The three fitting parameters in (1) specify the shape of the profile: parameter α defines the flatness of the profile at low latitudes; β the steepness of the profile at high latitudes; and γ the north-south asymmetry of the profile around the equator. For the case shown in Figure 1 the least squares fitting gives $\alpha = 1.081$, $\beta = 0.678$, $\gamma = 0.297$. Note that no echoes return in the lower latitude region of the path between the satellite location and its conjugate point. However, the total electron content can be calculated from the time delay of the first conjugate echo. The density distribution in this region is determined by assuming that the density gradients are continuous [*Huang et al.*, 2004].

[9] Since the purpose of this study is to develop an empirical model of the plasmaspheric densities, we use only measurements made inside the plasmasphere. IMAGE RPI passive measurements can be used to determine the location of the plasmapause and thus help to determine whether a plasmagram has been obtained from inside or outside of the plasmasphere. The RPI passive measurements are displayed in dynamic spectrograms (an example is displayed in Figure 2), in which a typical feature is the upper hybrid resonance (UHR) noise band. The UHR noise is a narrow band of signal enhancements bounded by the upper hybrid resonance frequency f_{uh} and electron plasma frequency f_{pe} [e.g., *Mosier et al.*, 1973; *Benson et al.*, 2004]. The plasmapause manifests as a dramatic change of the frequency of the UHR band in a short distance as seen on the dynamic spectrogram. Similar to the criterion adapted by *Carpenter and Anderson* [1992], we define the location where the density along the IMAGE orbit drops by at least a factor of 5 within $\Delta L < 0.5$ as the location where the plasmapause crossing occurred. For all 700 plasmagrams used in this study the corresponding dynamic spectrograms have been examined, with the aim of being certain that the measurements of the plasmagrams containing the invertible traces took place inside the plasmasphere.

[10] The size of the plasmasphere changes with geomagnetic activity. The location of the plasmapause can be as close as 2.5 R_E during intense magnetic storms and as far as beyond 7–8 R_E in periods of very quiet magnetic activities [e.g., *Carpenter and Anderson*, 1992; *Tu et al.*, 2007]. In the present study we restrict the measurements within $L = 4$. Data obtained beyond $L = 4$, particularly those in the low density plasmatrough region, will be analyzed in a future study. In Figure 3 we display the data coverage in a polar format of L – MLT. It is seen that the data coverage is rather uniform through all magnetic local times. Most of the measurements are located between $L = 2$ and $L = 4$, however 30 plasmagrams are obtained at closer distances (with $L = 1.62$ being the closest).

[11] The plasmapause location and structure display high variability [*Horwitz et al.*, 1990], and most often the body of the plasmasphere is confined within $L = 4$. While deriving a good plasmapause location/structure model is important, the active RPI sounding technique is not well suited to determine the locations of the plasmapause. It is rather rare to obtain a sequence of plasmagrams in the plasmasphere and plasmatrough with good invertible set of traces (which is

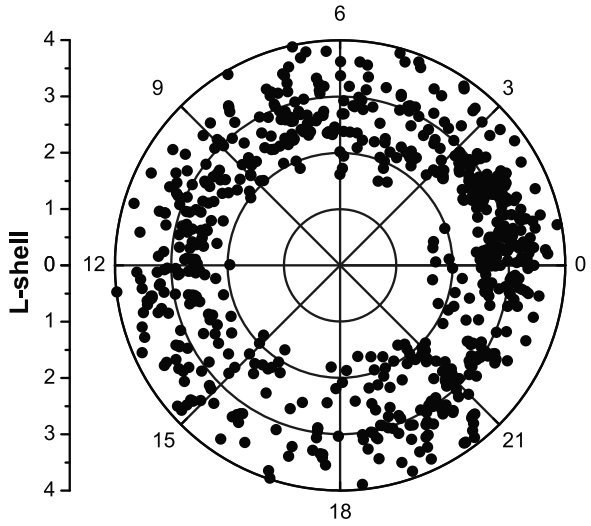

Figure 3. The *L*-shell – MLT coverage of the data set. Black circles represent the *L*-shell and magnetic local time of the measurements. Radial distance is equal to the *L*-shell value. Magnetic noon is to the left.

needed in order to determine the plasmapause crossing). A different kind of imaging (EUV) is better suited to study the shape and location of the plasmapause [*Goldstein et al.*, 2003]. Beyond $L = 4$, the RPI active sounding plasmagrams often become sporadic and difficult to invert. In other words, the MLT coverage beyond $L = 4$ is not as uniform as within it. Therefore, to avoid possible bias, we have limited our data selection within $L < 4$. Now let us examine whether the model can be used or extrapolated to beyond $L = 4$. Figure 10d shows the differences between the model predictions and the measurements made from the dynamic spectra in the region beyond $L = 4$. The relative errors are still less than 0.5 for about 80 percent of the data, similarly to Figure 10a that includes measurements from all *L*-shells. Therefore, although our model is based on the sounding measurements within $L = 4$, it can be used with confidence in the region beyond $L = 4$ up to the plasmapause. The location of the plasmapause is not included in our model; it may be derived according to previous models [e.g., *Carpenter and Anderson*, 1992; *O'Brien and Moldwin*, 2003].

[12] We have scaled and inverted 700 plasmagrams that were measured by the RPI in the years 2000–2005, which is half of a solar cycle. There are no plasmagrams with traces that can be inverted to derive the density profiles in year 2003 in the database, because the measurement programs were set for purposes other than active sounding of the plasmasphere. The resulting database consists of 500 density profiles from inversion of a single trace, 200 profiles from inversion of two traces (one in local hemisphere and another in conjugate hemisphere). Since each profile is based on many measurements along a field line, this adds up to more than 85,000 data points.

3. Model Development

[13] The model development is based on the functional form given by *Huang et al.* [2004; and further discussed in *Song et al.*, 2005; *Reinisch et al.*, 2004; *Tu et al.*, 2006]. For every profile a least squares fit of the equation (1) is performed and the fitting parameters (α, β, and γ) are determined. It is important to note that this fitting only determines the profile shape. The equatorial density N_{eq} is determined separately. When the satellite was not at the equator, the equatorial density could not be determined directly from observation. It can be interpolated when both local and conjugate traces are available or be extrapolated when only the local trace exists (knowing the fitting parameters). In the latter cases the asymmetry parameter γ cannot be constrained, since there is no rigorous method to determine the density in the conjugate hemisphere by knowing only the density in the local one, and thus the least squares fitting is done assuming $\gamma = 0$. It has been shown by *Tu et al.* [2006] that such fitting/extrapolation is reasonable and the extrapolated equatorial density is reliable. The values of equatorial density fall off exponentially with increasing *L*-shell as $10^{(A1-A2*L)}$ as can be seen in Figure 4a, where $A1 = 4.4693 \pm 0.0921$ and $A2 = 0.4903 \pm 0.0315$ (the uncertainties here and the remainder of the paper are defined by the standard errors times 1.96, which gives a 95% confidence interval). Additionally, we have attempted a power law fit, instead of exponential, to the equatorial densities measured by the RPI, which resulted in a $L^{-3.07}$ dependence. The exponential function produces a minimally greater correlation coefficient for our data set (0.76 versus 0.75).

[14] It is reasonable to assume that the *L*-shell is not the only parameter affecting the electron density distribution in the plasmasphere. Plasma in the plasmasphere is of ionospheric origin, and the diurnal variations of the ionosphere have been studied rather well over the course of many decades. Thus, the next dependence that we have attempted to quantify is the one on magnetic local time (MLT). After normalizing the equatorial densities to the model, the result has shown that the MLT dependence may be less than the level of fluctuations (see Figure 4b). If the data set is divided in two subsets (one with *L*-shell values less than 2.5 and another one with *L*-shell values greater than 2.5), the difference between noon and midnight densities becomes more pronounced for the smaller *L*-shells closer to the Earth. However, that difference is still less than the error of the averages, thus making it difficult to draw a conclusion. Additionally, dependence of the normalized equatorial densities on geomagnetic and solar activity indices (Kp, Dst, and F10.7) has not been observed either, possibly due to the insufficient data coverage at high levels of geomagnetic activity.

[15] After examining the equatorial densities, we now study the behavior of α, β, and γ. In general, the three fitting parameters may depend on *L*-value and/or local time. There is no obvious dependence of either α or β on the two variables, as can be seen from Figures 5 and 6. Therefore, we choose their average values, or $\alpha = 1.01 \pm 0.03$ and $\beta = 0.75 \pm 0.08$ as the representative values. We notice that due to the type of equation used to represent the density profile, α and β have some relationship. In other words, different pairs of α and β may produce similar profiles. We retested our result by first assuming a fixed $\alpha = 1.01$, making the formula double-parameter dependent, the average cosine power index β is found to be equal to 0.75, again relatively independent of either *L*-shell or magnetic local time. Such

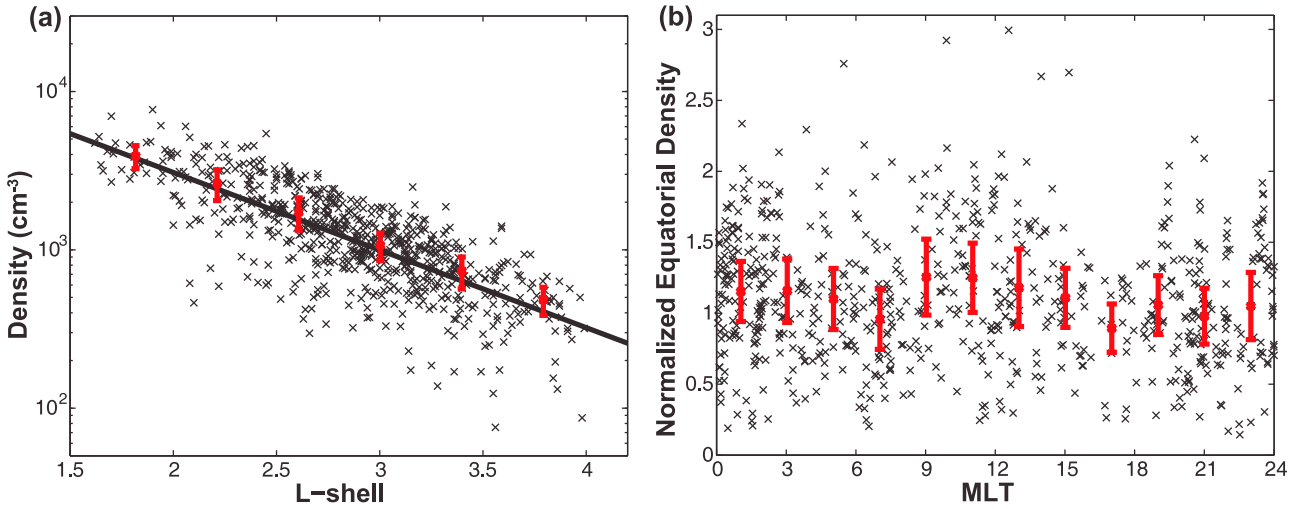

Figure 4. (a) Equatorial electron densities derived from the RPI measurements plotted as a function of *L*-shell. (b) Equatorial densities normalized by the RPI equatorial density model (second expression of equation (2)). The black line shows the best least squares fit to the measurements. The squares are binned averages, with red error bars displaying the statistical uncertainties.

values of $\alpha = 1.01 \pm 0.03$ and $\beta = 0.75 \pm 0.08$ are consistent with the results obtained by *Tu et al.* [2006] for case studies. Our current study is backing these values using a statistically significant number of 700 electron density profiles. It is worth noting that as the parameters are defined now, the steepness and the flatness of the field-aligned density profile are not dictated by the fixed parameters, since there is an invariant latitude (and thus *L*-shell) dependence in the cosine function.

[16] Analysis of the asymmetry parameter γ is limited to about 200 cases with both local and conjugate traces. Since the plasmasphere is directly connected to the ionosphere, seasonal density variations might be expected. However, our data set shows no obvious dependence (see Figure 7). γ varies around 0 (-0.04 ± 0.04) (meaning no statistically significant asymmetry), and no significant pattern in the variation (correlation coefficient less than 0.1) with either day of the year, magnetic local time, or *L*-shell. We recall that *Huang et al.* [2004] reported a case of asymmetry at solstice. They intuitively expected the asymmetry to be more pronounced at solstice as part of a seasonal control similar to effects observed in the ionosphere. However, multiple cases with very strong plasmasphere asymmetry occurring around equinoxes (with both foot points sunlit) have been found [*Ozhogin et al.*, 2009] during the analysis of the 200 plasmagrams, suggesting that the north-south asymmetry in the plasmaspheric density distribution is a consequence of dynamic processes, rather than of a seasonal variability. We further note that the functional form we use to study the asymmetry is most sensitive in high latitudes but not near the

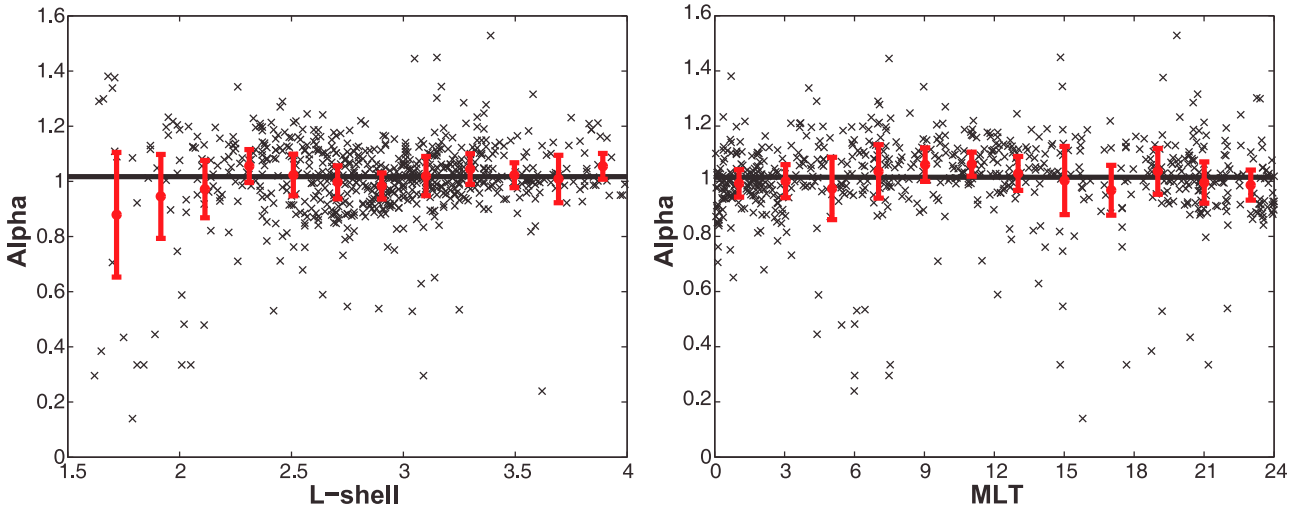

Figure 5. Values of the latitude flatness factor α versus (left) *L*-shell and (right) magnetic local time. The red squares indicate binned averages with the error bars displaying the statistical uncertainties. The straight black line is a constant value of 1.01.

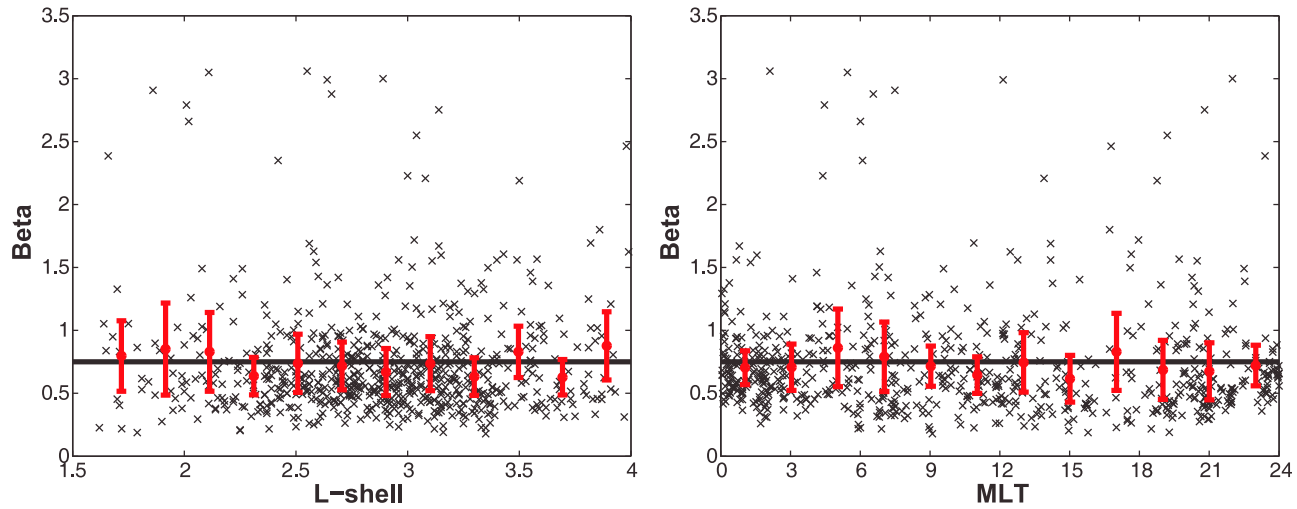

Figure 6. Values of the power index β versus (left) L-shell and (right) magnetic local time. The red squares indicate binned averages with the error bars displaying the statistical uncertainties. The straight black line is a constant value of 0.75.

equator. It is possible that a different functional form and a new approach are needed in future studies.

[17] The final result of the empirical plasmaspheric density model along a field line can be expressed as:

$$N(L,\lambda) = N_{eq}(L) \cdot \cos^{-(0.75\pm0.08)}\left(\frac{\pi}{2}\cdot\frac{(1.01\pm0.03)\lambda}{\lambda_{INV}}\right), \quad (2)$$
$$N_{eq}(L) = 10^{((4.4693\pm0.0921)-(0.4903\pm0.0315)\cdot L)},$$

where N_{eq} is the equatorial density and $\lambda < \arccos((8371/(L{*}R_E))^{-0.5})$ (this condition is to ensure that the model is applicable to altitudes above 2000 km).

4. Performance of the Plasmaspheric Density Models

4.1. Previous Models of the Plasmaspheric Number Density

[18] In order to evaluate the performance of our model it is necessary to compare it not only with the measured data, but also to the previous models. Here, we describe several relevant empirical models of plasmasphere densities. It is worth repeating that all of the previous models are based on in situ measurements, except for *Carpenter and Anderson*'s [1992] model part of which was derived from ground whistler observations. Furthermore, several models describe plasma densities not only in the plasmasphere, but also in the plasmatrough region; however, we compare only the modeled densities in the plasmasphere.

4.1.1. *Carpenter and Anderson* [1992], an ISEE/Whistler Model of Equatorial Electron Density in the Magnetosphere

[19]

$$\log_{10} n_e(L,D,S) = (-0.3145L + 3.9043) + \left[0.15\left(\cos\frac{2\pi(D+9)}{365} - 0.5\cos\frac{4\pi(D+9)}{365}\right) + 0.00127S - 0.0635\right]e^{-\frac{(L-2)}{1.5}}, \quad (3)$$

where D is the day number of the year, and S is the 13-month average sunspot number.

[20] This model describes the equatorial electron densities of the "saturated" plasmasphere. The first part of the model provides the "reference" profile and the second part describes the perturbation terms (annual, semiannual, and solar cycle variations) multiplied by the exponent to reflect the falloff with increasing L-shell value. The authors define the validity range of the model between L = 2.25 and the plasmapause inner limit (the inward boundary of the plasmapause).

4.1.2. *Gallagher et al.* [2000] Global Core Plasma Model

[21] This model uses a modified version of *Carpenter and Anderson*'s [1992] equation to describe the equatorial

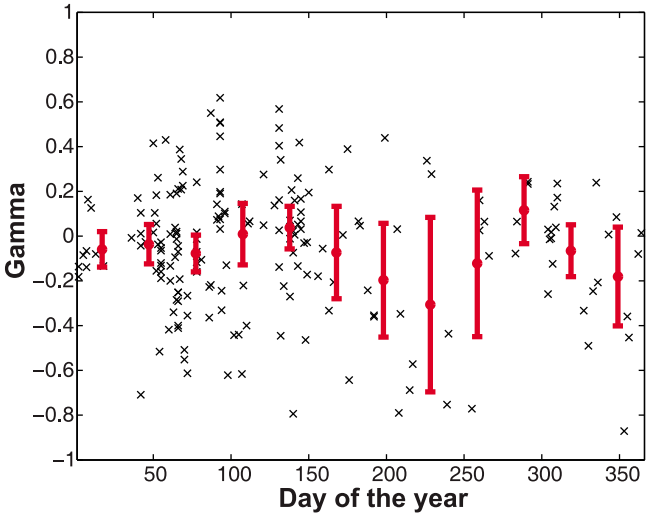

Figure 7. Values of the asymmetry parameter γ for cases with both local and conjugate traces, as a function of day of the year, display no seasonal variations. The red squares indicate binned averages with the error bars displaying the statistical uncertainties.

electron densities. While the second term remains intact, the first term is modified by using the measurements from the DE 1/RIMS instrument in the following way:

$$\log_{10} n_e(L,D,S) = (-0.79L + 5.3) + \left[0.15\left(\cos\frac{2\pi(D+9)}{365} - 0.5\cos\frac{4\pi(D+9)}{365}\right) + 0.00127S - 0.0635\right] e^{-\frac{(L-2)}{1.5}}. \quad (4)$$

The exponential function is used to interpolate between the topside ionosphere profile (provided by the International Reference Ionosphere (IRI) model [*Bilitza and Reinisch*, 2008]) and the plasmaspheric density profile:

$$n_e = e^{\frac{d}{d_0}+d_1}, \quad (5)$$

where d is the altitude in kilometers and d_0 and d_1 are fitting constants. The authors provide a FORTRAN code (http://plasmasphere.nasa.gov/models/).

4.1.3. *Sheeley et al.* [2001] Empirical Plasmasphere and Trough Density Model: CRRES Observations

[22] This model provides the electron density values for the L-shells between 3 and 7 as a power law function. Data from CRESS/SFR are averaged in bins of 1 L-shell by 1 h of local time, and the best fit curves for each L-shell are constructed, resulting in the following equation:

$$n_e(L) = 1390\left(\frac{3}{L}\right)^{4.83} \pm 440\left(\frac{3}{L}\right)^{3.60}. \quad (6)$$

Since the measurements come from the low-latitude portion of the plasmasphere, and the electron density is dependent strictly on L-shell without latitude factor, we take it as the equatorial density for the comparison purposes.

4.1.4. *Denton et al.* [2004, 2006] Electron Density in the Magnetosphere

[23]

$$\begin{aligned} n_e &= n_{e0}\left(\frac{R_{\max}}{R_G}\right)^A, \\ A &= A_{ne0} + A_{R_{\max}}, \\ A_{ne0} &= 6 - 3\log_{10} n_{e0} + 0.28(\log_{10} n_{e0})^2, \\ A_{R_{\max}} &= 2 - 0.43\left(\frac{R_{\max}}{R_E}\right), \end{aligned} \quad (7)$$

where $R_{\max}$ is the maximum geocentric radius R_G to any point on the field line, and n_{e0} is the value of n_e at $R_G = R_{\max}$ (magnetic equator). n_{e0} is an adapted version of *Carpenter and Anderson*'s [1992] equatorial density model, where the modification of the first term is obtained from the Polar/PWI measurements:

$$\log_{10} n_{e0}(R_{\max},S) = (-0.324R_{\max}/R_E + 3.78) + [0.00127S - 0.0635]e^{-\frac{(R_{\max}/R_E-2)}{1.5}}, \quad (8)$$

where S is the 13-month average sunspot number. For a dipole magnetic field, $R_{\max} = LR_E$ and, thus, the electron densities can be rewritten as $n_e = n_{e0}(\cos(\lambda))^{-2A}$ where λ is the magnetic latitude. Typical values of A for the plasmasphere are found to be between 0 and 1. However, in a more recent version [*Denton et al.*, 2006] the authors suggest using $A \sim 1$ for the plasmasphere. The model is applicable under the following condition: $2.5\ R_E \le R_{\max} \le 8.5\ R_E$, $2\ R_E \le R_G \le R_{\max}$, and $2 \le n_{e0} \le 1500\ \text{cm}^{-3}$.

[24] This section is by no means an exhaustive review of the existing plasmasphere models, since it is not a purpose of this paper. We choose these four representative models to compare the results with our model and the RPI measurements. Since *Carpenter and Anderson*'s [1992], and *Sheeley et al.*'s [2001] models do not have latitudinal dependence, they are used only for the equatorial densities comparison. *Gallagher et al.*'s [2000] model provides the variation of density with the altitude, due to the exponential function used, thus making a full comparison possible. Finally, *Denton et al.*'s [2006] model has the latitudinal dependence, and we compare the results within the range and density limitations of their model.

4.2. Comparison of Equatorial Density Models

[25] Before we compare the models, let us make a general comment on empirical model development. First, the number of fitting parameters: clearly, more fitting parameters, as we often see in empirical models which introduce a large number of fitting parameters without adequate justification, provide more flexibility in a model to describe more complicated situations or dependences. However, the statistical significance or robustness of the model decreases if the total number of the data points is limited. Second, the functional form: the objective for choosing a particular functional form for a fitting is to reduce the number of terms in approaching the underlying pattern of the data set. In principle, the theory of statistics can determine the "right" number of parameters, as long as the observation parameters are measured or determined with equal level of accuracy and sensitivity; this is not the case here. Our model is looking for increased robustness, rather than flexibility, thus it is more important to have fewer parameters. In theory one can choose either a Taylor series or Fourier series, each of which is able to describe any variation. The issue is the efficiency or the speed of the convergence. A better chosen functional form can catch a variation with a small number of terms leaving small room for further improvement by adding more terms.

[26] Now, we compare various empirical models of equatorial densities, examine the differences between the RPI model and previous models, and discuss possible causes for the differences. Previous studies inferred equatorial densities either from the ground whistler measurements or from in situ measurements which might have been made at various latitudes along the satellite orbits. In the latter situation, the measurements representing the densities on the same field line but at different latitudes are most likely obtained with large time separations during which the solar wind and magnetospheric conditions most likely had changed. In contrast, because of the unique ability of the RPI to make almost instantaneous density measurements along the magnetic field line, we are able to determine equatorial densities with high precision even when the satellite is not at the equator. In the cases of successful inversion of plasmagrams with both field-aligned traces the equatorial density

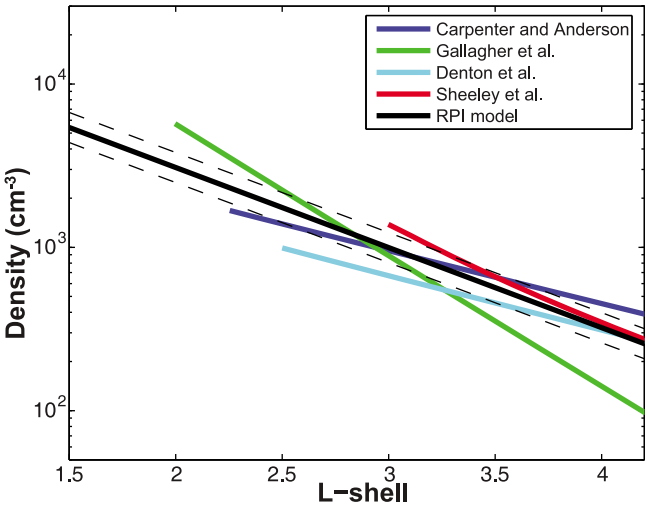

Figure 8. Comparison of equatorial density models. The black solid line is the model from the present study (dashed lines represent statistical uncertainties), the blue line is the model of *Carpenter and Anderson* [1992] (applicability range: L-shell > 2.25), the green line is the model of *Gallagher et al.* [2000] ($L > 2$), the cyan line is the model of *Denton et al.* [2006] ($L > 2.5$), and the red line is the model of *Sheeley et al.* [2001] ($L > 3$).

value, although not directly measured, is interpolated under the constraints of the measurements (the total plasma content from the satellite location to its conjugate point) and the assumption of the continuity of the density gradient. These determinations are highly accurate [*Reinisch et al.,* 2001]. For the cases where only one trace can be successfully inverted, we extrapolate the density profile to the equator, based on the functional form given in the first expression of equation (2). It is worth mentioning that both scenarios lead to practically identical equatorial density equations.

[27] Figure 8 compares the newly developed plasmasphere model to the principal parts of the previous models. All five of these models have been obtained using different instruments on different satellites, under different solar conditions, and of course different methods were used to infer the equatorial densities. Additionally, various magnetic field models have been used, which can lead to additional deviations in results. Thus, differences are unavoidable, but they are not dramatic, especially at distances greater than $L = 3$, and are mostly within the statistical uncertainties. The RPI model lies between the models of *Gallagher et al.* [2000] and *Carpenter and Anderson* [1992]. Let us discuss the possible explanations of the differences in the results.

[28] First of all, *Sheeley et al.* [2001] use the data from CRRES's sweep frequency receiver with the upper frequency limit of 400 kHz, which results in the maximum possible density reading of 1984 cm^{-3}, limiting the model to the outer plasmasphere. The authors set the lower boundary of their model to be at $L = 3$. As we move further away from the Earth, the difference between the RPI model and the model of *Sheeley et al.* [2001] decreases. Another possible source of differences might be within the method of separating the plasmasphere from the plasmatrough. While we have manually selected our data to ensure that the measurements were made within the plasmasphere by the method described in the section 2, *Sheeley et al.* [2001] have used an artificially defined criterion: density at plasmapause = 10 $(6.6/L)^4$, to determine the plasmapause location. However, the potential selection biases should only lead to lower predicted density values in the plasmasphere (and higher values in the plasmatrough).

[29] Next, the model of *Carpenter and Anderson* [1992] includes the effects of the annual/semiannual variations and solar cycle, which were derived from many years of ground whistler measurements, while our model does not. The result of these effects can be seen in Figure 4b of *Carpenter and Anderson* [1992]. However, we do not see such dependencies statistically significant in our data set (possibly due to the insufficient length of the mission in the case of solar cycle effects). The works of *Gallagher et al.* [2000] and *Denton et al.* [2004] implement the same dependencies without modifications (except that *Denton et al.* [2004] includes only the solar cycle variations, omitting the semi-annual and annual variations terms). We think that the potential users of our model may consider adding the same expressions to the equatorial density formula, if they wish to. In other words, the approach of *Sheeley et al.* [2001] is closer to ours: we do not drop the additional (semi-annual, annual, and solar cycle) terms, since we do not have them to begin with, we just do not include them from *Carpenter and Anderson* [1992]. In order to have a level comparison, we consider only the terms in the first parenthesis (principal part) in equation (3) for this qualitative comparison. It can be seen from Figure 8 that this model is rather close to the present RPI model. The relatively small differences are most likely caused by the selection of the data for the models. *Carpenter and Anderson* [1992] modeled the saturated plasmasphere, under very quiet geomagnetic conditions, while we neither limit the data selection to any particular geomagnetic disturbance level nor make the distinction between saturated and any other state of the plasmasphere. Additionally, the 25 profiles they used to derive the principal part of equation (3) were not all strictly equatorial, but within ~30° magnetic latitude, which may have affected the resulting L-shell dependence.

[30] Further, the model of *Gallagher et al.* [2000] has the steepest slope of all models. The authors have used data from the DE 1/RIMS instrument, and have limited the selection to the extended quiet conditions (3-day weighted $K_P < 1.3$), however all local times and, more importantly, all latitudes are included. It is possible that the data set includes measurements from outside of the plasmapause, thus explaining the steepness of the slope.

[31] Finally, the model of *Denton et al.* [2004] displays a slope of the line very similar to the one of *Carpenter and Anderson* [1992], but predicts lower densities overall. In addition, the method used to infer the equatorial densities is much different from ours and is based on the assumption that the Polar satellite crosses the same magnetic field line twice. There is a possibility that the reason for systematically lower predicted densities is that Polar measurements were taken during solar minimum (March 1996–September 1997). However, the model also describes the field-aligned density distribution, which we will discuss in the next section.

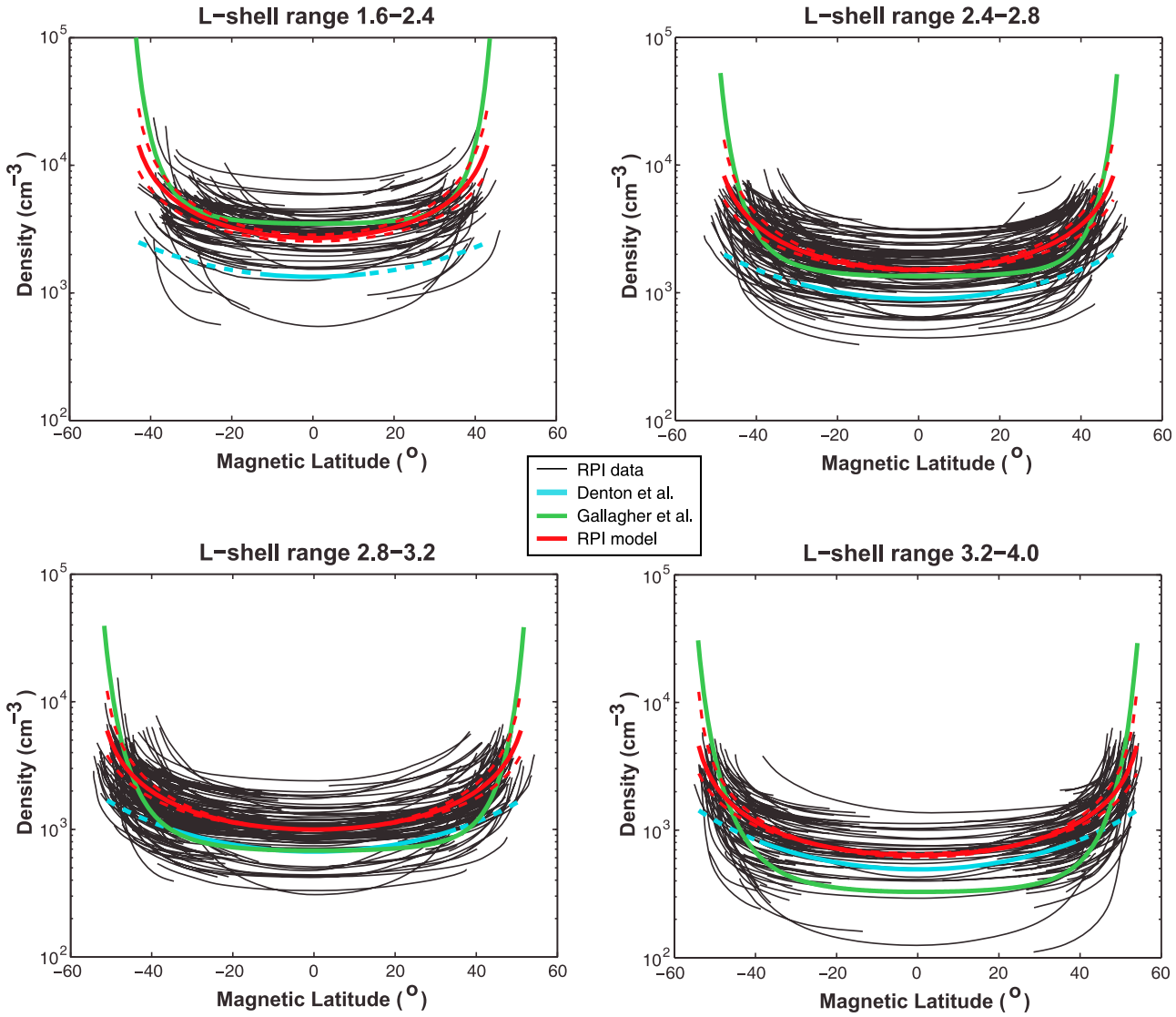

Figure 9. Measured RPI electron density profiles (black lines) separated in 4 *L*-shell bins. Red line is the RPI model (dashed red lines represent statistical uncertainties), cyan line is the model of *Denton et al.* [2006] (the line is dashed when R < 2 R_E), and green line is the model of *Gallagher et al.* [2000].

4.3. Field-Aligned Density Comparison

[32] In addition to the equatorial densities, another important part of the developed plasmaspheric density model is the latitudinal dependence of plasmaspheric densities. The latitudinal variations of the density profiles are large and differ from case to case. An empirical model can only catch the overall shape with a functional form that builds on the L-value dependence.

[33] We bin the RPI data according to the *L*-shell in 4 bins: *L*-shell value between 1.6 and 2.4, 2.4 and 2.8, 2.8 and 3.2, and, finally, 3.2 and 4.0. The spacing is not uniform, due to the uneven distribution of the available echo traces. By varying the bin size, we can achieve a comparable number of profiles in each bin.

[34] Figure 9 displays the binned RPI profiles and the three models that provide the latitudinal dependences. The main purpose of Figure 9 is to qualitatively compare the models and the data and study the general behavior and correspondence of models to the data. It is important to choose the model parameters correctly in order to plot the model profiles that are representative of the profiles in each bin. First, since the distribution of profiles within each bin is not uniform, we select the *L*-shell value for the models to be equal to the median value of *L*-shells of the profiles in each bin (2.12, 2.63, 3.00, and 3.40, respectively). Next, the boundary of the model is important. The lower boundary of applicability range of our model (∼2000 km) is selected rather conservatively. In reality, almost a quarter of the 700 density profiles used in this study extend to altitudes lower than 2000 km, thus the model applicability range can be extended if needed; however, the uncertainties do increase with decreasing altitude, as can be seen from Figure 9. Distinct outlier traces with significantly higher density values at lower altitudes can be seen at the edges of each panel. In order to properly compare the correspondence of models to the data, the models are plotted in the range of $\pm(\lambda_{INV} - 3^\circ)$. It can be noticed that fewer traces in the first bin

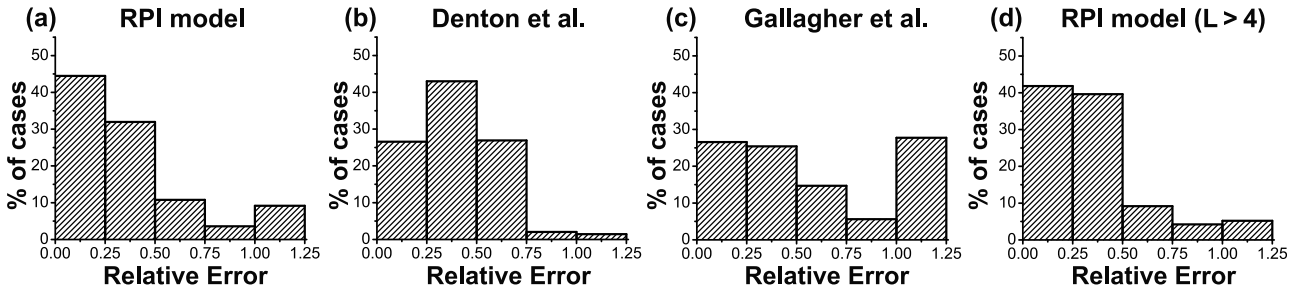

Figure 10. The histograms of relative errors for the three models: (a) the RPI model, (b) the model of *Denton et al.* [2006], (c) the model of *Gallagher et al.* [2000], and (d) the RPI model for $L > 4$. The last bins indicate the sum of all the cases with relative errors greater than 1.

extend to such low altitudes. The reasons for that are the following: first, the traces on the plasmagrams do not always extend through the whole frequency band. Second, depending on the sounding program, the upper frequency limits differ. As a result, different profiles reach different minimal altitudes. When the satellite is at low L-shells (first bin), the densities are high, and the traces often reach the maximum sounding frequency, thus limiting the maximum density reading.

[35] Since the model of *Denton et al.* [2006] includes the solar cycle dependence, we have chosen the $S = 78$, which is the average value of the sunspot number for the years of the IMAGE mission (2000–2005). The plasmaspheric part of the model of *Gallagher et al.* [2000] has annual and semi-annual variations, in addition to the solar cycle dependence. The function has a minimum at day 173, and two maxima: at days 052 and 295. In order to study the general behavior of the model, we average the results from the minimum and maximum values. It is worth noting that the difference in equatorial densities between just the principal part and the principal plus solar cycle variations (with $S = 78$) is very small: 4 percent at $L = 3$, and it decreases with increasing distance. Similarly to *Denton et al.* [2004] and *Gallagher et al.* [2000], who do not plot the seasonal and solar cycle effects in their papers, we plot only principal parts of the equatorial densities in Figure 8 to avoid confusion. However, these effects play larger role as we move away from the equator. For example, the model of *Gallagher et al.* [2000] shows a rather significant change of densities at high latitudes with seasons (likely due to the connection to the IRI model, which has a strong seasonal dependence), and such averaging is appropriate for a qualitative comparison (Figure 9). The value of the index of geomagnetic activity K_P is chosen to be equal to 2, since it is the average value in the time intervals that the RPI measurements were made.

[36] The model of *Denton et al.* [2006] produces a steeper profile at high altitudes, with A set to 1, than with A dependent on the distance and equatorial density (see equation (7)). However, the densities do not increase quickly enough at lower altitudes (less than 2 R_E, which is the lower boundary of the data coverage of that model) to capture the change in the measured profile. Even though the equations for the RPI model and the model of *Denton et al.* [2006] look somewhat similar, there is a significant difference in the behavior. While the profile produced by *Denton et al.* [2006] ($n_e = n_{e0}(\cos(\lambda))^{-2A}$) becomes steeper with the increase of the parameter A (which is equal to $\sim$1 in the plasmasphere), the RPI modeled densities ($n_e = n_{eq}(\cos((\pi/2)1.01\lambda/\lambda_{INV}))^{-0.75}$) rise more quickly as the magnetic latitude approaches the invariant latitude. Such fast increase in the density is seen in the measured density profiles. Note that parameter λ_{INV} implicitly includes dependence of L in a dipole field.

[37] In contrast, the model of *Gallagher et al.* [2000] displays a very sharp density increase at high latitudes, resulting in significant over-estimations at low altitudes. This increase is created by the exponential function that connects the ionospheric densities, which are obtained from the IRI model, to the equatorial plasmaspheric densities. Connecting the bottomside ionospheric measurements or models to the plasmasphere is a very complicated, important, and active research topic. A slower increase of density with latitude by the use of exponential function would cause an unrealistic density gradient at the connection point. It is possible that a more complicated function (e.g., Vary-Chap function) is needed to describe the change in density from the F2 peak to the plasmasphere [*Reinisch et al.*, 2007; *Nsumei et al.*, 2012].

[38] After the qualitative comparison, we compare the models quantitatively. To do this, a rather rigorous approach is taken. The models are taken in their full form without any omissions. Since every density profile consists of many measurements, we can calculate the relative error for every point. A relative error is defined as the absolute value of the difference between the density measured by RPI and modeled value, normalized by the measured density. The results are plotted (Figure 10) as histograms, with the bin width of 0.25 in relative error. It can be seen that the RPI model results in nearly 45% of the modeled values having the relative error being less than 0.25, while the other two models have same relative errors only for 26% of the cases. Furthermore, greater than three quarters of all RPI model values have a relative error less than 0.5.

[39] The last bin is the sum of all relative errors greater than 1. That number is very low for the model of *Denton et al.* [2006], since it systematically under-estimates the measured densities, since if the modeled value is less than measured, the relative error is always less than 1. The opposite can be seen with the model of *Gallagher et al.* [2000]; since it often over-estimates, especially at high latitudes, it has more than a quarter of cases with a relative error greater than 1.

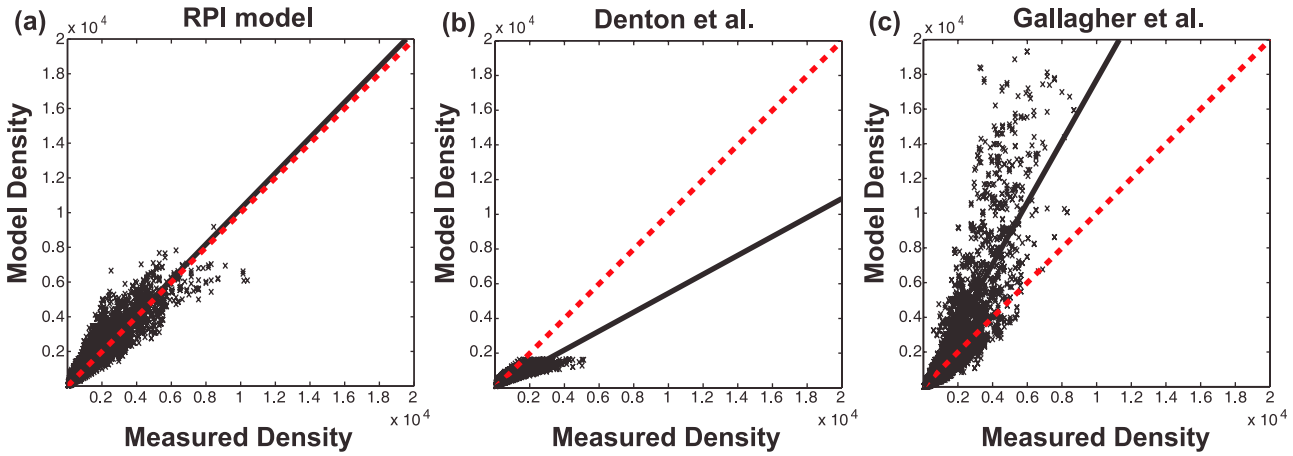

Figure 11. Measured densities plotted against modeled values for the (a) RPI model, (b) the model of *Denton et al.* [2006], and (c) the model of *Gallagher et al.* [2000]. Red dashed line ($y = x$) indicates perfect match. The black lines are the least squares fits ($y = a*x$) to the data. The corresponding values of a are: 1.02, 0.55, and 1.77. And the corresponding correlation coefficients are: 0.91, 0.86, and 0.75.

4.4. Comparison With Dynamic Spectrum

[40] The comparison of the equatorial density and latitudinal profiles among different models may arguably be unfair to other models because the RPI model is developed from the RPI data and should better represent the data. Next we compare the performance with the passive measurements made by the RPI. Note that this is an independent test, since the passive in situ measurements were made independently (in time and location) from the active measurements and have not been used in the development of the present model. All three models are tested on equal footing.

[41] We have compared the three models to the densities derived from the dynamic spectrograms during 113 plasmaspheric fly throughs. The total number of density measurements is greater than 1600, however when comparing the results to the model of *Denton et al.* [2006] a lesser number is used due to the application range of $R > 2\ R_E$ for that model. The results are shown in Figure 11. In cases when the modeled value equals the measured value exactly, the data points would be on the red dashed diagonal line ($y = x$). Even though some scattering exists, when a least squares fit is applied to the data (black line), one can see that it coincides with the red dashed line almost perfectly for the RPI model. As for the models of *Denton et al.* [2006] and *Gallagher et al.* [2000], the outcome is similar to the comparison with the measured field-aligned profiles. While the former model tends to under-estimate, the latter one over-estimates.

5. Discussion and Summary

[42] The proposed empirical model describes plasmaspheric densities as a function of L-shell and magnetic latitude. For simplicity and convenience, without significant loss in accuracy, equation (2) can be rewritten as:

$$N(L,\lambda) = N_{eq}(L) \cdot \cos^{-0.75}\left(\frac{\pi}{2}\cdot\frac{\lambda}{\lambda_{INV}}\right), \qquad (9)$$
$$N_{eq}(L) = 10^{(4.4693-0.4903\cdot L)}.$$

While the equatorial density from the formula is not dramatically different from that calculated with the previous models, the major difference lies in the field-aligned distribution. The dependence on magnetic latitude creates density gradients that have significant consequences in physical processes in this region. We are able to model the plasmaspheric densities down to the altitudes of ~2000 km with a single formula. We choose only the traces that were obtained within the plasmasphere for this analysis. Determination of the plasmapause location is done by studying the corresponding dynamic spectrogram.

[43] As mentioned previously, the lower boundary is set rather conservatively and the upper boundary, the plasmapause, is stricter. In principle, there is a possibility that the location of the plasmapause affects the distribution of the density within the plasmasphere. However, there is no significant evidence that the distribution of the plasmaspheric density changes with the plasmapause distance from the Earth. In other words, if we measure the equatorial density at $L = 2.5$, it will likely be the same regardless whether the plasmapause is at $L = 3.5$ or $L = 4.5$, unless other conditions have changed. It can be seen from the comparison of the dynamic spectra from different satellite passes or superposed density measurements at the equator [e.g., *Carpenter and Anderson*, 1992, Figures 1 and 3]. If such dependency exists, it would be captured by our model on average, since we did not limit the selection of profiles based on the plasmapause location.

[44] The model is based on the remote sensing measurements in active mode and consistent with measured field-aligned density profiles. For 76 percents of the measurements the relative error is found to be within 0.5. Its performance has been tested against the in situ measurements made by the RPI in passive mode. Although the magnetic latitude and L-shell are not the only variables determining the plasma density, we have found them dominant in determining the density profiles. During case studies, one can observe variation and evolution of the density profiles with time of the day, or before, after, and during a storm. However, profile shape in general is found statistically to be only weakly, if

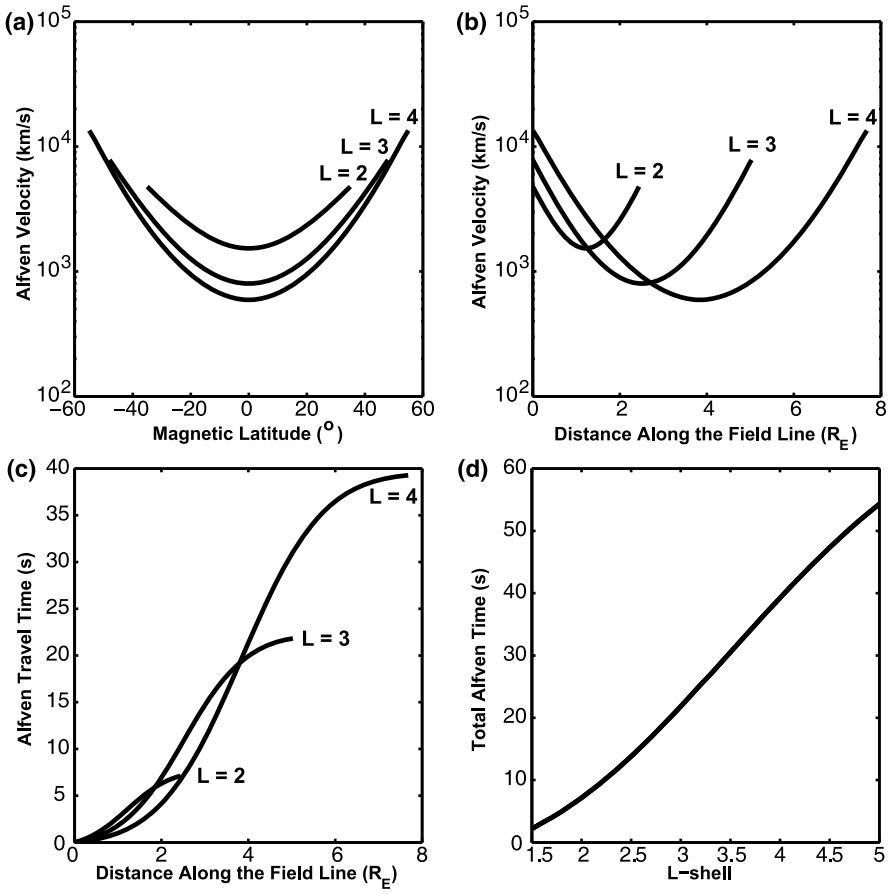

Figure 12. Alfven velocity along the magnetic field line at L = 2, 3, and 4 as a function of (a) magnetic latitude and (b) distance along the field line. (c) Alfven travel time as a function of distance along the field line and (d) total Alfven propagation time from one hemisphere to another as a function of L-shell. All calculations go from 2000 km altitude in southern hemisphere to 2000 km altitude in northern, along the magnetic field line.

any, dependent of either magnetic local time or geomagnetic activity. The equatorial density model of *Carpenter and Anderson* [1992] includes the dependence on the solar cycle, as well as annual and semi-annual variations, derived from many years of ground whistler measurements. These effects have been included similarly by *Gallagher et al.* [2000] and to some extent by *Denton et al.* [2006]. In our analysis, these factors appear to be secondary compared to the normal fluctuations after the L-value and latitudinal effects are removed.

[45] The plasmasphere is a rather complicated entity, influenced not only by the ionosphere, but the sun and geomagnetic activity as well. Diffusive equilibrium would dictate that the plasma density should be almost constant along the magnetic field line near the equator. However, the density profiles obtained from the RPI active measurements clearly show that this is rarely the case.

[46] As the plasmasphere is constantly changing, and is affected by several intertwined processes, such as ionospheric up-flow or down-flow, depletion and refilling during the disturbed times, our data shows that the equatorial densities fall off following the exponential law, not the power law (if a power law fit is chosen, the densities vary as $L^{-3.07}$). The model that we suggest also produces the change in the density around the equator that varies with L-shell. At L = 4 the density increases by 30% at $\pm$30 degrees of magnetic latitude, compared with the equatorial values. As L-shell decreases, the latitudinal variation becomes even more significant: the densities at $\pm$30 degrees are double the densities at the equator of the field line with L = 1.9.

[47] The model developed in the present study has the potential for wide applications. An example is the ability to calculate the typical Alfven velocities and propagation times in the plasmasphere. Although in the presence of heavy ions the Alfven velocity depends on their concentration and distribution, Figure 12 shows the Alfven velocity assuming the absence of heavy ions. Knowing the density and the magnetic field we can calculate first Alfven velocities and then propagation times by integration along the magnetic field lines (see Figure 12) within the range of applicability of the model (above $\sim$2000 km). The Alfven speed increases from around 1000 km/s in the equator to 10,000 km/s near the Earth as the field strength increases. Similarly, smaller L-shells support greater Alfven speed. The Alfven time combines the effect of the Alfven speed and the length of the field. Since the contribution from below 2000 km altitude to the Alfven time is small, the Alfven time derived using our model from above 2000 km may be taken as the Alfven

wave propagation time which is from few seconds at small L-shells to close to 1 min near the plasmapause.

[48] We acknowledge that the comparison is made using the measurements based on which this present model is developed and previous models were developed based on other measurements, and that there is a perceived potential bias toward the present model. However, if the plasmasphere behaves according to the same set of underlying physical processes and each of the databases is large enough and statistically representative of these processes, when the uncertainties are included in the consideration, the overall quality of representation of the physical processes from each model can be assessed. A comparison of the model with the plasma density data obtained from other satellites (ISEE, CRRES, CLUSTER, and Polar) has been initiated, and will be reported in a future study.

[49] In summary, we have developed an empirical plasmaspheric density model that appropriately represents the plasma densities obtained from the RPI active sounding and passive measurements. It does not show a density increase at the equator, since such behavior has not been observed in neither active nor passive RPI measurements. Based on the comparisons of the modeled density from the RPI and previous models, we show that the newly developed RPI model provides an improved description of the latitude dependence of the plasmaspheric density along the magnetic field lines with significantly fewer adjustable parameters. This model has the potential to be used in studying plasma wave propagation in the plasmasphere and provide the background plasmaspheric density distribution for investigating the wave-particle interaction and radiation belt dynamics.

[50] **Acknowledgments.** This work was supported by the NSF grants ATM-0902965 and AGS-0903777 to the University of Massachusetts Lowell. UML's CORPRAL plasmagram prospecting software and NASA Virtual Wave Observatory were instrumental in selection of plasmagrams for our investigation. Product ID for RPI plasmagram data is http://spase.info/VWO/DisplayData/IMAGE/RPI/IMAGE_RPI_PNG_PGM_PT5M. Dst and solar wind/IMF data were obtained from WDC for Geomagnetism (Kyoto) and CDAWeb system, respectively. We thank G. Khmyrov, A. Kozlov, I. Galkin, R. Denton, and D. Gallagher for valuable discussions.

[51] Masaki Fujimoto thanks the reviewers for their assistance in evaluating this paper.

References

Angerami, J. J., and J. O. Thomas (1964), Studies of planetary atmospheres: 1. The distribution of electrons and ions in the Earth's exosphere, *J. Geophys. Res.*, *69*(21), 4537–4560, doi:10.1029/JZ069i021p04537.

Benson, R. F., P. A. Webb, J. L. Green, L. Garcia, and B. W. Reinisch (2004), Magnetospheric electron densities inferred from upper-hybrid band emissions, *Geophys. Res. Lett.*, *31*, L20803, doi:10.1029/2004GL020847.

Bilitza, D., and B. W. Reinisch (2008), International Reference Ionosphere 2007: Improvements and new parameters, *Adv. Space Res.*, *42*, 599–609, doi:10.1016/j.asr.2007.07.048.

Binsack, J. H. (1967), Plasmapause observations with the M.I.T. experiment on IMP 2, *J. Geophys. Res.*, *72*(21), 5231–5237, doi:10.1029/JZ072i021p05231.

Burch, J. L. (2000), IMAGE mission overview, *Space Sci. Rev.*, *91*(1–2), 1–14, doi:10.1023/A:1005245323115.

Carpenter, D., and R. Anderson (1992), An ISEE/whistler model of equatorial electron density in the magnetosphere, *J. Geophys. Res.*, *97*(A2), 1097–1108, doi:10.1029/91JA01548.

Denton, R. E., J. Goldstein, and J. D. Menietti (2002), Field line dependence of magnetospheric electron density, *Geophys. Res. Lett.*, *29*(24), 2205, doi:10.1029/2002GL015963.

Denton, R. E., J. D. Menietti, J. Goldstein, S. L. Young, and R. R. Anderson (2004), Electron density in the magnetosphere, *J. Geophys. Res.*, *109*, A09215, doi:10.1029/2003JA010245.

Denton, R. E., K. Takahashi, I. A. Galkin, P. A. Nsumei, X. Huang, B. W. Reinisch, R. R. Anderson, M. K. Sleeper, and W. J. Hughes (2006), Distribution of density along magnetospheric field lines, *J. Geophys. Res.*, *111*, A04213, doi:10.1029/2005JA011414.

Fung, S. F., and J. L. Green (2005), Modeling of field-aligned guided echoes in the plasmasphere, *J. Geophys. Res.*, *110*, A01210, doi:10.1029/2004JA010658.

Galkin, I. A., G. M. Khmyrov, A. V. Kozlov, and B. W. Reinisch (2008), Intelligent resident archive for RPI Level 2 data, in *Radio Sounding and Plasma Physics*, *AIP Conf. Proc.*, *974*, 111–117, doi:10.1063/1.2885020.

Gallagher, D. L., P. D. Craven, and R. H. Comfort (1988), An empirical model of the Earth's plasmasphere, *Adv. Space Res.*, *8*, 15–24, doi:10.1016/0273-1177(88)90258-X.

Gallagher, D. L., P. D. Craven, and R. H. Comfort (1998), A simple model of magnetospheric trough total density, *J. Geophys. Res.*, *103*, 9293–9297, doi:10.1029/97JA03665.

Gallagher, D. L., P. D. Craven, and R. H. Comfort (2000), Global core plasma model, *J. Geophys. Res.*, *105*, 18,819–18,833, doi:10.1029/1999JA000241.

Goldstein, J., R. E. Denton, M. K. Hudson, E. G. Miftakhova, S. L. Young, J. D. Menietti, and D. L. Gallagher (2001), Latitudinal density dependence of magnetic field lines inferred from Polar plasma wave data, *J. Geophys. Res.*, *106*(A4), 6195–6201, doi:10.1029/2000JA000068.

Goldstein, J., M. Spasojevic, P. H. Reiff, B. R. Sandel, W. T. Forrester, D. L. Gallagher, and B. W. Reinisch (2003), Identifying the plasmapause in IMAGE EUV data using IMAGE RPI in situ steep density gradients, *J. Geophys. Res.*, *108*(A4), 1147, doi:10.1029/2002JA009475.

Gurnett, D. A., et al. (1995), The Polar plasma wave instrument, *Space Sci. Rev.*, *71*, 597–622, doi:10.1007/BF00751343.

Horwitz, J. L., R. H. Comfort, and C. R. Chappel (1990), A statistical characterization of plasmasphere density structure and boundary locations, *J. Geophys. Res.*, *95*(A6), 7937–7947, doi:10.1029/JA095iA06p07937.

Huang, X., and B. W. Reinisch (1982), Automatic calculation of electron density profiles from digital ionograms: 2. True height inversion of topside ionograms with the profile-fitting method, *Radio Sci.*, *17*(4), 837–844, doi:10.1029/RS017i004p00837.

Huang, X., B. W. Reinisch, P. Song, P. Nsumei, J. L. Green, and D. L. Gallagher (2004), Developing an empirical density model of the plasmasphere using IMAGE/RPI observations, *Adv. Space Res.*, *33*, 829–832, doi:10.1016/j.asr.2003.07.007.

Larsen, B. A., D. M. Klumpar, and C. Gurgiolo (2007), Correlation between plasmapause position and solar wind parameters, *J. Atmos. Sol. Terr. Phys.*, *69*(3), 334–340, doi:10.1016/j.jastp.2006.06.017.

Lawrence, D. J., M. F. Thomsen, J. E. Borovsky, and D. J. McComas (1999), Measurements of early and late time plasmasphere refilling as observed from geosynchronous orbit, *J. Geophys. Res.*, *104*, 14,691–14,704, doi:10.1029/1998JA900087.

Moldwin, M. B., L. Downward, H. K. Rassoul, R. Amin, and R. R. Anderson (2002), A new model of the location of the plasmapause: CRRES results, *J. Geophys. Res.*, *107*(A11), 1339, doi:10.1029/2001JA009211.

Mosier, S. R., M. L. Kaiser, and L. W. Brown (1973), Observations of noise bands associated with the upper hybrid resonance by the IMP 6 radio astronomy experiment, *J. Geophys. Res.*, *78*, 1673–1679, doi:10.1029/JA078i010p01673.

Nsumei, P., B. W. Reinisch, X. Huang, and D. Bilitza (2012), New Vary-Chap profile of the topside ionosphere electron density distribution for use with the IRI Model and the GIRO real time data, *Radio Sci.*, *47*, RS0L16, doi:10.1029/2012RS004989.

O'Brien, T. P., and M. B. Moldwin (2003), Empirical plasmapause models from magnetic indices, *Geophys. Res. Lett.*, *30*(4), 1152, doi:10.1029/2002GL016007.

Ozhogin, P., J. Tu, P. Song, and B. W. Reinisch (2009), North-south asymmetry of the plasmaspheric densities: Observations from the IMAGE Radio Plasma Imager, *Eos Trans. AGU*, *90*(52), Fall Meet. Suppl., Abstract SM11A-1565.

Rasmussen, C. E., S. M. Guiter, and S. G. Thomas (1993), A two-dimensional model of the plasmasphere: Refilling time constants, *Planet. Space Sci.*, *41*(1), 35–43, doi:10.1016/0032-0633(93)90015-T.

Reinisch, B. W., and W. Huang (1983), Automatic calculation of electron density profiles from digital ionograms: 3. Processing of bottomside ionograms, *Radio Sci.*, *18*, 477, doi:10.1029/RS018i003p00477.

Reinisch, B. W., et al. (2000), The Radio Plasma Imager investigation on the IMAGE spacecraft, *Space Sci. Rev.*, *91*, 319–359, doi:10.1023/A:1005252602159.

Reinisch, B. W., X. Huang, P. Song, G. S. Sales, S. F. Fung, J. L. Green, D. L. Gallagher, and V. M. Vasyliunas (2001), Plasma density distribution

along the magnetospheric field: RPI observations from IMAGE, *Geophys. Res. Lett.*, *28*, 4521–4524, doi:10.1029/2001GL013684.

Reinisch, B. W., X. Huang, P. Song, J. L. Green, S. F. Fung, V. M. Vasyliunas, D. L. Gallagher, and B. R. Sandel (2004), Plasmaspheric mass loss and refilling as a result of a magnetic storm, *J. Geophys. Res.*, *109*, A01202, doi:10.1029/2003JA009948.

Reinisch, B. W., P. Nsumei, X. Huang, and D. K. Bilitza (2007), Modeling the F2 topside and plasmasphere for IRI using IMAGE/RPI and ISIS data, *Adv. Space Res.*, *39*, 731–738, doi:10.1016/j.asr.2006.05.032.

Reinisch, B. W., M. B. Moldwin, R. E. Denton, D. L. Gallagher, H. Matsui, V. Pierrard, and J. Tu (2009), Augmented empirical models of plasmaspheric density and electric field using IMAGE and Cluster data, *Space Sci. Rev.*, *145*, 231–261, doi:10.1007/s11214-008-9481-6.

Sheeley, B., M. Moldwin, H. Rassoul, and R. Anderson (2001), An empirical plasmasphere and trough density model: CRRES observations, *J. Geophys. Res.*, *106*(A11), 25,631–25,641, doi:10.1029/2000JA000286.

Singh, N., and J. L. Horwitz (1992), Plasmasphere refilling: Recent observations and modeling, *J. Geophys. Res.*, *97*, 1049–1079, doi:10.1029/91JA02602.

Siscoe, G., D. Baker, R. Weigel, J. Hughes, and H. Spence (2004), Roles of empirical modeling within CISM, *J. Atmos. Sol. Terr. Phys.*, *66*(15–16), 1481–1489, doi:10.1016/j.jastp.2004.03.028.

Song, P., B. W. Reinisch, X. Huang, and J. L. Green (2005), Magnetospheric active wave experiments, in *Frontiers of Magnetospheric Plasma Physics*, *COSPAR Colloq. Ser.*, *16*, 235–246, doi:10.1016/S0964-2749(05)80036-8.

Tsyganenko, N. A. (2002), A model of magnetosphere with a dawn-dusk asymmetry: 2. Parameterization and fitting to observations, *J. Geophys. Res.*, *107*(A8), 1176, doi:10.1029/2001JA000220.

Tu, J., P. Song, B. W. Reinisch, J. L. Green, and X. Huang (2006), Empirical specification of field-aligned plasma density profiles for plasmasphere refilling, *J. Geophys. Res.*, *111*, A06216, doi:10.1029/2005JA011582.

Tu, J., P. Song, B. W. Reinisch, and J. L. Green (2007), Smooth electron density transition from plasmasphere to the subauroral region, *J. Geophys. Res.*, *112*, A05227, doi:10.1029/2007JA012298.